ISSN 1063-7761, Journal of Experimental and Theoretical Physics, 2017, Vol. 125, No. 3, pp. 451–464. © Pleiades Publishing, Inc., 2017.
Original Russian Text © V.V. Brazhkin, E. Bychkov, O.B. Tsiok, 2017, published in Zhurnal Eksperimental'noi i Teoreticheskoi Fiziki, 2017, Vol. 152, No. 3, pp. 530–546.

SOLIDS AND LIQUIDS

High-Precision Measurements of the Compressibility and the Electrical Resistivity of Bulk g-As_2Te_3 Glasses at a Hydrostatic Pressure up to 8.5 GPa

V. V. Brazhkin[a]*, E. Bychkov[b], and O. B. Tsiok[a]

[a] *Vereshchagin Institute of High-Pressure Physics, Troitsk, Moscow, 108840 Russia*
[b] *LPCA, UMR 8101 CNRS, Université du Littoral, Dunkerque, 59140 France*
**e-mail: brazhkin@hppi.troitsk.ru*

Received March 7, 2017

Abstract—High-precision studies of the volume and the electrical resistivity of g-As_2Te_3 glasses at a high hydrostatic pressure up to 8.5 GPa at room temperature are performed. The glasses exhibit elastic behavior in compression only at a pressure up to 1 GPa, and a diffuse structural transformation and inelastic density relaxation (logarithmic in time) begin at higher pressures. When the pressure increases further, the relaxation rate passes through a sharp maximum at 2.5 GPa, which is accompanied by softening the relaxing bulk modulus, and then decreases, being noticeable up to the maximum pressure. When pressure is relieved, an unusual inflection point is observed in the baric dependence of the bulk modulus near 4 GPa. The polyamorphic transformation is only partly reversible and the residual densification after pressure release is 2%. In compression, the electrical resistivity of the g-As_2Te_3 glasses decreases exponentially with increasing pressure (at a pressure up to 2 GPa); then, it decreases faster by almost three orders of magnitude in the pressure range 2–3.5 GPa. At a pressure of 5 GPa, the electrical resistivity reaches 10^{-3} Ω cm, which is characteristic of a metallic state; this resistivity continues to decrease with increasing pressure and reaches 1.7×10^{-4} Ω cm at 8.1 GPa. The reverse metal–semiconductor transition occurs at a pressure of 3 GPa when pressure is relieved. When the pressure is decreased to atmospheric pressure, the electrical resistivity of the glasses is below the initial pressure by two–three orders of magnitude. Under normal conditions, both the volume and the electrical resistivity relax to quasi-equilibrium values in several months. Comparative structural and Raman spectroscopy investigations demonstrate that the glasses subjected to high pressure have the maximum chemical order. The glasses with a higher order have a lower electrical resistivity. The polyamorphism in the As_2Te_3 glasses is caused by both structural changes and chemical ordering. The g-As_2Te_3 compound is the first example of glasses, where the reversible metallization under pressure has been studied under hydrostatic conditions.

DOI: 10.1134/S1063776117080155

1. INTRODUCTION

Tellurium-based chalcogenide glasses are important technological materials and are widely used for memory elements and in infrared photonics [1]. Binary As–Te glasses serve as model objects. However, the structures of the short- and intermediate-range orders even in these binary glasses are still incompletely clear, which hinders an analysis of their characteristics using a structure–property correlation [2–15]. The g-As_2Te_3 glasses are intermediate compounds between conventional easily vitrifying chalcogenide glasses and metallic glasses, which require ultrafast cooling for their formation. Similarly to the Te melt, the As_2Te_3 melt is a metal at a small overheating above the melting temperature [16, 17], and its crystallization upon cooling can only be avoided at a cooling rate higher than 100 K/s. It was considered in early works that the structure of g-As_2Te_3 is analogous to the structure of the classic ideal random network, which is similar to the As_2S_3 glass network based on corner-sharing trigonal $AsX_{3/2}$ pyramids [2]. However, it was found later [3–12] that the short-range order of the g-As_2Te_3 glass differs strongly from that of the corresponding crystalline phase and is characterized by a very strong chemical disorder (30–60%), in contrast to the "classic" g-As_2S_3, where the chemical disorder does not exceed 3–5% (i.e., it is lower by an order of magnitude). The chemical disorder is determined as the ratio of the number of homopolar As–As bonds to the total number of bonds. Moreover, the structure and properties of g-As_2Te_3 glasses depend strongly on the melt temperature and the quenching rate, which also hinders their investigation [8, 15]. Unfortunately,

an adequate model of the structures of the short- and intermediate-range orders in the g-As_2Te_3 glass is still absent.

The g-As_2Te_3 glasses have a small optical semiconductor gap (about 0.8 eV) and a low activation energy (about 0.4 eV) in transport measurements, which makes this system attractive for studying glass metallization during compression (in particular, glasses are not shunted by the pressure-transmitting medium in measurements). Among the stoichiometric chalcogenide glasses, only the g-As_2Te_3 glasses undergo metallization at a pressure lower than 10 GPa, which makes it possible to study bulk samples under purely hydrostatic conditions [18]. Nevertheless, g-As_2Te_3 was studied under pressure in a few works. The deposition of thin amorphous a-As_2Te_3 films, the properties of which can differ substantially from those of the bulk glass, has been mainly investigated. The metallization of a-As_2Te_3 films was detected at a pressure of 10 GPa: the metallization in [19] was accompanied by crystallization, and the metallization in occurs with a retained amorphous state [20]. The metallic phase of amorphous a-As_2Te_3 films exhibited superconductivity, which was studied in a number of works (see, e.g., [21]). The electrical resistivity of bulk g-As_2Te_3 glasses was investigated at a pressure up to 6.5 GPa only in [22]. All investigations of the electrical resistivity of a-As_2Te_3 and g-As_2Te_3 at a pressure higher than 1 GPa were carried out under nonhydrostatic conditions [19, 20, 22]. The electrical resistivity of g-As_2Te_3 glasses under hydrostatic conditions was only studied in [23] but to a pressure of 0.9 GPa. It is interesting that g-As_2Te_3 is a rare example of the glasses the glass transition temperature and the crystallization temperature of which decrease rapidly (2–3 K/kbar) with increasing pressure [24].

The structure and other properties of the g-As_2Te_3 glasses, including their compressibility (which is a fundamental characteristic), have not been studied earlier due to many factors, including the difficulty of fabrication of unstrained pore-free glass samples. Since the structure of the g-As_2Te_3 glasses differs strongly from a simple ideal network of the g-As_2S_3 type, nontrivial behavior of compressibility and other characteristics during compression can be expected.

The purpose of this work is to study the compressibility, the relaxation processes, and the electrical resistivity of g-As_2Te_3 glasses at a high accuracy, a pressure up to 8.5 GPa, and room temperature under ideal hydrostatic conditions and to estimate the structure and the dynamics of the glasses under normal conditions.

2. EXPERIMENTAL

The initial glasses were prepared from elementary As (99.9999%) and Te (99.997%) (Aldirch Chemical Ltd.). The substances were placed in preliminarily cleaned quartz tubes with an inside diameter of 8 mm, which were pumped out and hermetically sealed. The melts were held and stirred at 600°C for 6 h and were then water quenched. The initial ingots had pores several tens of microns in size; they made it impossible to measure the compressibility if additional measures were not taken, since microcracks appeared in samples at a pressure of 0.7–1.2 GPa. Therefore, the glass samples had to be subjected to additional treatment to heal pores and to remove a heterogeneous chemical order.

A strong dependence of the structure and the chemical order on the annealing temperature in glassy arsenic telluride was demonstrated in [8, 15]. The stoichiometric As_2Te_3 glass is characterized by a high susceptibility to crystallization. It was found that the softening and crystallization of the glass occurred in a very narrow temperature range: noticeable softening (glass could be formed by hot pressing) began at 130–135°C, and intense crystallization upon heating at a rate of 1 K/min began at 145°C with a heat release peak at 165.5°C. We experimentally found the following thermobaric treatment conditions to fabricate pore-free samples with crystalline phase impurities. Initial glass samples in an ampule with a quasi-hydrostatic medium were placed in a mold preliminarily heated to 141.9°C, the pressure was then rapidly increased to 0.2 GPa, the mold was cooled with water, and the pressure was relieved. The samples were heated to 135–136°C under pressure, and the total time of holding the samples at above 130°C was about 3 min. To illustrate the required accuracy of parameters, we note that about 0.5% crystalline phase formed in a sample at 138°C.

Comparative structural and Raman studies were performed for the following three groups of glasses under normal conditions: the quenched glasses are the initial glasses after melt quenching, the hot-pressed glasses are the samples after thermobaric treatment at 136°C and 0.2 GPa, and the glasses after high pressure are the samples subjected to experiments at a maximum pressure of 8.2–8.4 GPa.

Neutron diffraction experiments were carried out on the SANDALS diffractometer of the ISIS Pulsed Neutron Source at the Rutherford–Appleton Laboratory (United Kingdom) [25]. The low-energy neutron resonances at Te limited the available region of scattering vectors $Q = 4\pi\sin(\theta/\lambda)$, where 2θ is the scattering angle for neutron wavelength λ, to 25 $Å^{-1}$. Diffraction data were corrected for the scattering of the diffractometer with a container, self-absorption, multiple scattering, and inelastic scattering [26]. As a result, total neutron structure factor $S_N(Q)$ was obtained.

Experiments on high-energy X-ray diffraction were performed on the 6-ID-D station of the Advanced Photon Source (Argonne National Laboratory, United States) [27]. The X-ray photon energy was 100.329 keV, which ensured the available region of

scattering vectors Q up to 30 Å^{-1}. A two-dimensional PerkinElmer model 1621 detector was used to record X-ray diffraction patterns of samples. X-ray diffraction (XRD) data were analyzed with the Fit2D software package [28]. To obtain full X-ray structure factor $S_X(Q)$, we used standard procedures, which included the subtraction of the background spectrum of the detector and corrections for the detector geometry, different efficiencies of the detector elements, self-absorption, and Compton scattering [29, 30].

Raman spectra were measured on a LabRam HR (Horiba Jobin Yvon) Raman microscope–spectrometer using coherent radiation at a wavelength of 785 nm. Since the glassy compound As_2Te_3 is easily melted and crystallized under a laser beam [8], the solid-state laser diode power was limited to 200–300 μW. A chosen region on the sample surface was controlled before and after Raman measurements and no changes were observed. The measurements were performed at three–four sites to achieve reliable results.

The fabricated pore-free glass samples had a density of 5.55 g/cm^3. All glass samples, namely, the quenched glasses, the hot-pressed glasses, and the glasses after high-pressure experiments had the typical structure of glass and did not contain crystalline phase impurities (Fig. 1). The samples for measurements under pressure were parallelepipeds with faceted edges. Samples 3 × 2 × 1.5 mm^3 in size were used for compressibility measurements, and samples 2.5 × 1 × 0.7 mm^3 in size were used for electrical resistivity measurements.

High-pressure experiments were carried out a Toroid-type apparatus with a central pip diameter of 15 mm [31]. The volume of a glass sample under hydrostatic pressure conditions was measured using the tensometric technique from [32]. The absolute accuracy of measuring the volume by this technique is 0.2% and its sensitivity is 10^{-3}%. The important advantage of this technique is a very short measurement time (0.2 s). As a result, comprehensive information on the behavior of sample volume under pressure can be obtained. Moreover, this technique can be used to study the kinetics of the pressure-induced change in the sample volume in a wide time range of 10–10^7 s. Another important advantage of the technique is the fact that the baric dependences of the sample volume can be obtained when pressure increases and decreases under purely hydrostatic conditions. This technique was successfully applied earlier to study both oxide and chalcogenide glasses (see, e.g., [33, 34]).

As the pressure-transmitting medium, we used a methanol–ethanol (4 : 1) mixture with a hydrostatic limit of about 10 GPa. The pressure was measured by a manganin transducer calibrated against the transitions in bismuth (2.54 and 7.7 GPa). The reproducibility of the pressure scale in all experiments (possibility of comparing the results of different experiments at the same pressure) was 3 MPa.

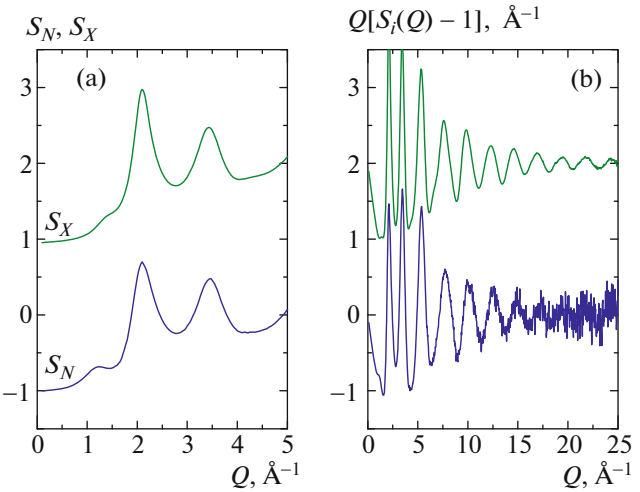

Fig. 1. (Color online) (a) X-ray ($S_X(Q)$) and neutron ($S_N(Q)$) structure factors at low scattering vectors $Q \le 5$ Å^{-1} and (b) reduced structure factors $Q[S_i(Q) - 1]$, where $i = N$ or X, at $Q \le 25$ Å^{-1} for glassy As_2Te_3. The neutron structure factor is given for the quenched glass, and the X-ray structure factor is given for the glass subjected to a high hydrostatic pressure of 8.3 GPa.

When the glass densification kinetics was studied at a fixed pressure, it was maintained at a certain level accurate to ±2 MPa.

The electrical resistances of glasses were measured by the four-probe method. Contacts were soldered using an experimental low-melting-point solder, namely, the three-component In–Bi–Sn eutectic (3 : 1 : 1 in atomic fractions). As was found later, Field's alloy has a close composition. The soldering iron tip was made of a eutectic Ag–Cu alloy (72 at % Ag). Soldering was carried out at a temperature of about 70°C. Moreover, a saturated (at room temperature) solution of indium in gallium was used as a solder to measure the electrical resistances of relaxed samples after pressure release. Soldering was performed at room temperature and measurements were conducted using liquid contacts. The electrical resistivity was obtained by dividing the electrical resistance by the initial sample sizes. The possible error of calculating the electrical resistivity was controlled by the inaccuracy of determining the geometric factor of the sample and was estimated at ±10%.

3. RESULTS

The sample volume was measured when the pressure was continuously increased at a rate of 0.07–0.12 GPa/min or continuously decreased at a rate of 0.03–0.05 GPa/min. To plot baric dependences, we took the points obtained at a pressure step of 0.025 GPa, which allowed us to plot an almost continuous curve without interpolation. Figure 2 shows the

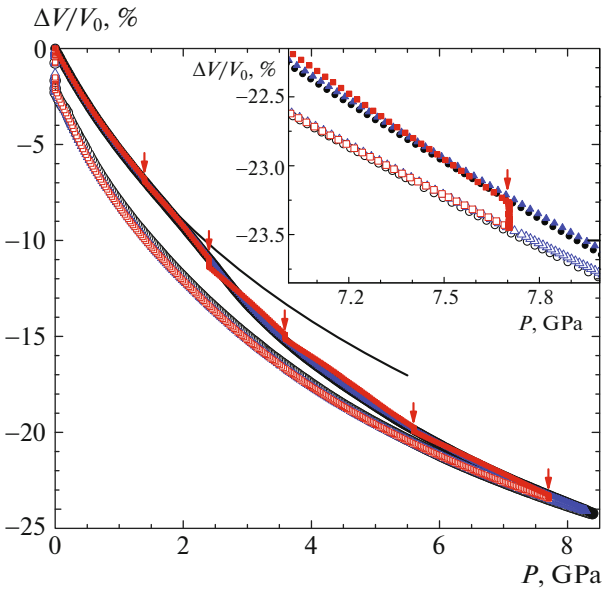

Fig. 2. (Color online) Baric dependences of the volume of the hot-pressed g-As_2Te_3 glass for (solid symbols) increasing and (open symbols) decreasing pressure. The results of three experiments are shown. In one of the experiments, we studied the glass densification kinetics at a fixed pressure at the points indicated by arrows. The solid line was plotted by fitting the initial segments (0–1.2 GPa) of the $V(P)$ dependence by the Murnaghan equation ($B_0 = 15.8 \pm 0.15$, $dB/dP = 6.1 \pm 0.2$). (inset) Enlarged region near the maximum pressure, where the densification kinetics was studied on one sample.

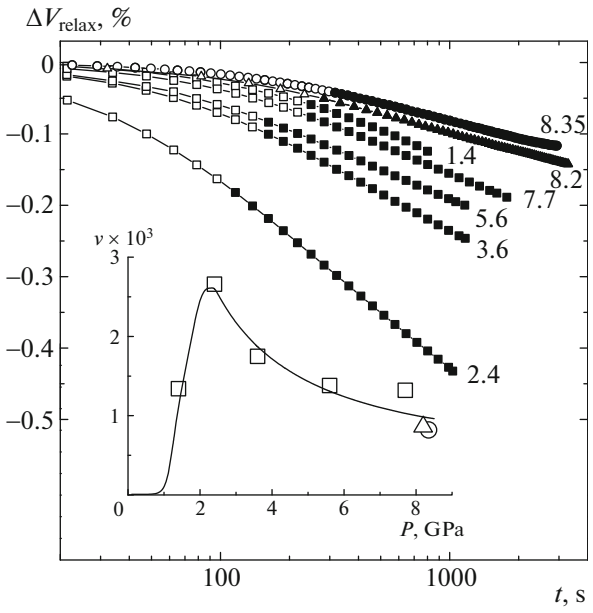

Fig. 3. Relaxation of the g-As_2Te_3 glass volume at a fixed pressure. The numerals at the curves correspond to the pressure in gigapascals. (inset) Relaxation rate vs. pressure, which was determined as $\nu = -d(V/V_0)/d(\log t)$ in the linear segment of the time dependences (solid symbols).

baric dependences of the glass g-As_2Te_3 volume for three samples. The compression curves are seen not to be approximated by a simple general equation of state, and elastic behavior is only observed to a pressure of 1 GPa. In the pressure range 2–3.5 GPa, the decrease in the volume is anomalous, and the additional increase in the density as compared to the continuation of the compression curve at the same modulus is approximately 2% during this diffuse transformation. The pressure hysteresis between the compression and unloading curves as compared to other chalcogenide glasses is small, the residual densification does not exceed 2%, and the volume relaxes to the initial value in several months under normal conditions. To demonstrate the measurement accuracy, we present segments of the baric dependences of the glass volume near the maximum pressure in the inset to Fig. 2. Relaxation measurements were conduced on one of the samples at several fixed pressures. It is seen that the baric dependences of all three samples coincide with each other at a high accuracy (about 0.1%) and that, after isobaric relaxation, the compression curve during the subsequent increase in the pressure merges asymptotically with the compression curve where relaxation measurements were absent.

At pressures above 1 GPa, the volume of the g-As_2Te_3 glass depends substantially on time at a fixed pressure (relaxation), and the change in the volume at long times is proportional to the logarithm of time (Fig. 3). The deviation from a logarithmic dependence in the initial segment is related to a finite rate of increase of pressure in the experiment, and the processes with a relaxation time shorter than 100–300 s are partly or fully completed at the stage of increase of pressure before holding. The relaxation rate has a sharp maximum at 2.5 GPa (inset to Fig. 3), and the absolute value of the maximum relaxation intensity is close to the corresponding maximum values for $GeSe_2$ glasses, which exhibit a change in the type of connection of structural tetrahedra from edge-sharing connection to corner-sharing connection and a transition to an easily compressible network in a narrow pressure range [34].

The high sensitivity of the tensometric technique makes it possible to find the effective bulk compression moduli of glasses by direct point-by-point differentiation without additional processing. Figure 4 shows the pressure dependences of the bulk moduli of the g-As_2Te_3 glasses. These moduli are seen to grow linearly with pressure up to 1 GPa. In the initial section, the bulk modulus is $B = 15.8 \pm 0.15$ GPa and its derivative with respect to pressure is $dB/dP = 6.1 \pm 0.2$. The bulk modulus of the g-As_2Te_3 glass has not been measured earlier. The following values are available for other arsenic-based chalcogenide glasses:

$B = 14.5$ GPa for g-As_2Se_3 glasses and $B = 13.3$ GPa for g-As_2S_3 glasses [18]. When the pressure increases further, derivative dB/dP decreases and becomes negative (softening of the modulus). This is accompanied by intense volume relaxation up to the highest pressure. The bulk modulus in this range corresponds to relaxing values. The difference between the relaxing and relaxed bulk moduli indicate the presence of activation processes and diffuse transformations in the glasses [33–35]. The softening of the relaxing modulus is maximal at 2.5 GPa, i.e., at the pressure of the maximum relaxation rate. After long-term isobaric relaxation, the effective bulk modulus during a further increase in the pressure first corresponds to high relaxed values and, then, decreases to the effective relaxing values corresponding to the curve for a constant rate of loading (modulus "forgets" the history; see Fig. 4). The small irregularities in the relaxing modulus reproduce the variations of the rate of change of pressure in the relaxation range. At a pressure above 4.5 GPa, the slope of the baric dependence of the effective bulk modulus decreases in compression (additional softening of the modulus), which is likely to be due to the appearance of new relaxation processes. The rate of relaxation levels off during isobaric measurements after the rapid decrease in the pressure range from 2.5 to 3.6 GPa.

When pressure is relieved, the glasses behave elastically up to 1.5 GPa and the bulk modulus corresponds to relaxed values. At lower pressures, the effective bulk modulus decreases more intensely, which is related to the relaxation processes that occur during the reverse transformation (which is not completed down to atmospheric pressure). It is interesting that, when the pressure decreases, the baric dependence of the relaxed bulk modulus has an inflection point at 4 GPa and dB/dP decreases from 8 to 5.5. This behavior of the relaxed bulk modulus during a decrease in the pressure has not been detected for other glasses. When the pressure is decreased, the bulk moduli of the g-As_2Te_3 glasses are close to the moduli after isobaric relaxation at the stage of increasing pressure, which points to the same structure of the short-range order in these glasses at the stages of increasing and decreasing pressure (see Fig. 4). When the structures of the short-range order in glasses at the same pressure do not coincide at the stages of increasing and decreasing pressure, it is evident that their relaxed moduli do not coincide with each other (see the discussion in [34, 35]).

Figure 5 shows the effective bulk moduli of the g-As_2Te_3 glasses as a function of density. The following unexpected effect has been revealed: the bulk moduli are almost coincident at the stages of increasing and decreasing pressure in the density range 6.55–6.7 g/cm^3, and these moduli diverge at lower and higher densities. This confluence of bulk modulus curves has not been observed earlier for other glasses.

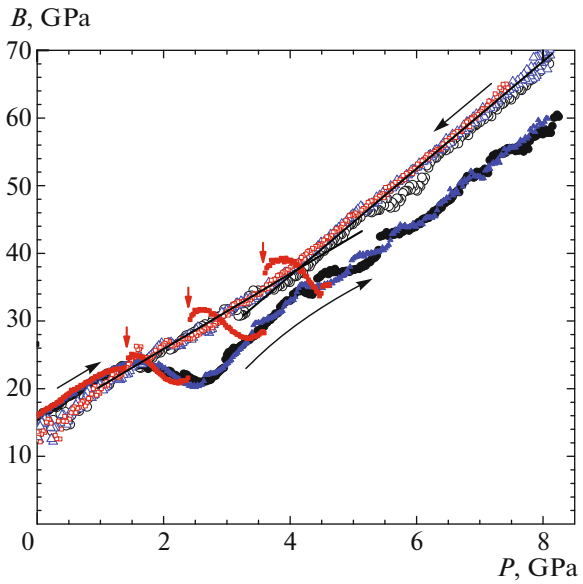

Fig. 4. (Color online) Apparent bulk moduli of the g-As_2Te_3 glass that were obtained from the initial $V(P)$ data as $B = -V(dP/dV)_T$ for (solid symbols) increasing and (open symbols) decreasing pressure. The solid curves emphasize the inflection point in the baric dependence of the bulk modulus when pressure decreases. The colors and symbols used to present the results of different experiments correspond to the designations in the $V(P)$ curves in Fig. 2. The vertical arrows indicate the points at which the time dependences of the volume were measured in one experiment.

The curves in Fig. 5 exhibit several clear relaxation stages (apparently, relaxation channels) in the g-As_2Te_3 glass at high pressures.

Figure 6 depicts the baric dependences of the electrical resistivities of the glasses. Both the quenched and hot-pressed samples were studied. The initial electrical resistivities (at $T = 25$°C) of the hot-pressed glasses 1.25×10^3 Ω cm) are an order of magnitude lower than those of the quenched glasses (1×10^4 Ω cm). The electrical resistivities of the glasses decrease exponentially when the pressure increases to 1.5–2 GPa. At $P <$ 0.4 GPa, the shunting of a sample by the pressure-transmitting medium in the quenched glass becomes important (Fig. 6, dashed curve). Above 2 GPa, the rate of decrease of the electrical resistivity increases sharply: it decreases by almost three orders of magnitude in the narrow pressure range 2–3.5 GPa (where the most pronounced volume changes were observed). At a pressure above 3 GPa, the baric dependences of the electrical conductivities of different types of glasses merge into one dependence. The difference between the absolute values of the electrical resistivities of various samples with different histories does not exceed 10% at the maximum pressure, which corresponds to the absolute accuracy of measurements. We can conclude that a transition into the metallic state takes

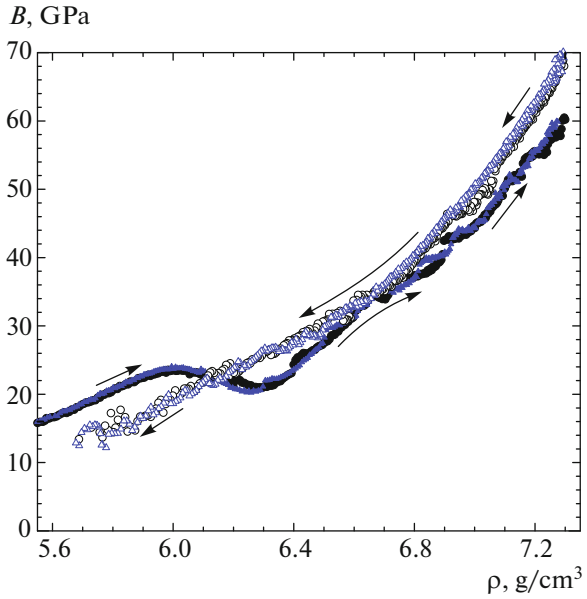

Fig. 5. (Color online) Apparent bulk moduli of the g-As_2Te_3 glass for (solid symbols) increasing and (open symbols) decreasing pressure for two experiments, which were calculated from the initial data as functions of the sample density. The colors and symbols of different experiments correspond to the designations in Figs. 2 and 4.

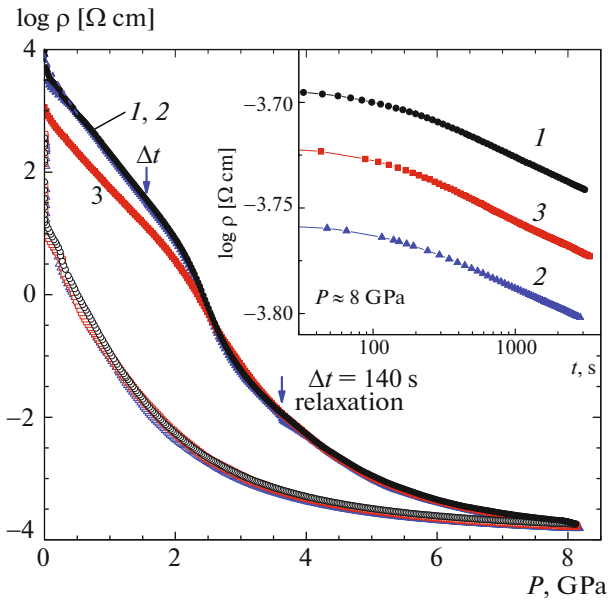

Fig. 6. (Color online) Baric dependences of the electrical resistivity of glassy g-As_2Te_3 for (solid symbols) increasing and (open symbols) decreasing pressure. The results of three experiments are shown. Experiments *1* and *2* were performed on the initial quenched glass samples, and experiment *3*, on the hot-pressed sample. In experiment *2*, two short stops were made at 1.5 and 3.5 GPa (indicated by arrows) to estimate the kinetics. (inset) Kinetics of changing the electrical resistivity at the maximum pressure (steady-state conditions are indicated by solid symbols). The curves were obtained by projecting experimental points onto line $P = 8$ GPa along the slope measured in decreasing pressure ($d(\log\rho)/dP = -0.0555$).

place at a pressure of 5 GPa with allowance for the fact that the characteristic electrical resistivities for the minimum metallic conductivity of chalcogenide glasses are $(1–2) \times 10^{-3}$ Ω cm (Mott criterion) [36].

Apart from the Mott criterion of the minimum conductivity, the data from [20] also point to the metallic state. Based on the temperature dependences of the electrical resistivity at various pressures, the authors of [20] concluded that the semiconductor gap decreased almost linearly to zero at high pressures. However, those measurements were performed at a very high error and the pressure of metallization was overestimated almost twofold. The baric dependences of the electrical resistivity and the volume are absolutely smooth; therefore, we can assume that metallization is smooth and crystallization does not occur. A single noticeable effect in this pressure range is the inflection point in the baric dependence of the relaxing modulus (see Fig. 4). Metallization is assumed to accelerate structural relaxation due to a decrease in the potential barriers to atomic jumps between various local configurations. During further compression, the electrical resistivity continues to decrease slowly and becomes 1.7×10^{-4} Ω cm at 8.1 GPa. As in the case of volume, the electrical resistivity exhibits time-logarithmic relaxation up to the maximum pressure (see the inset to Fig. 6). A 1% change in the volume in the relaxation dependences at the maximum pressure corresponds to an approximately twofold increase in the electrical conductivity. The reverse metal–insulator transition takes place at 3 GPa when the pressure is relieved. After pressure release, the electrical resistivities of the samples were lower than those of the initial hot-pressed and quenched samples by two and three orders of magnitude, respectively, in spite of the fact the residual densification was only 2% (Fig. 6).

For comparison, Fig. 7 shows the reported data obtained for g-As_2Te_3 amorphous films and bulk g-As_2Te_3 glasses under nonhydrostatic conditions along with the data obtained for one of the quenched samples. It is seen that the earlier measurements were performed at a high error, which is likely to be related to both the influence of strong shear stresses and the problems of forming reliable contacts (most measurements in [22] were carried out using the two-probe scheme). The baric dependences on decreasing pressure were also measured at a very high error in [20], which can be related to both nonhydrostatic conditions and bad calibration of the chamber in the reverse run.

Long-term holding after pressure release under normal conditions is accompanied by an increase in the electrical resistivity by 1.5–2 (!) orders of magnitude, which results in the values that are characteristic

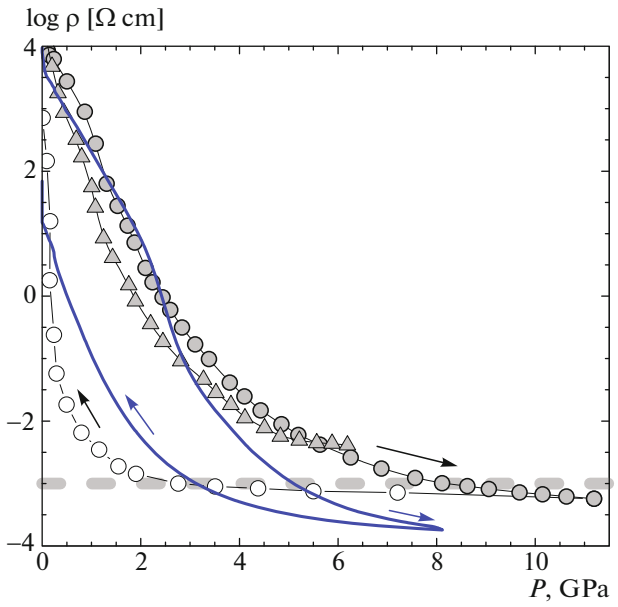

Fig. 7. (Color online) Reported data for the electrical resistivity of the g-As_2Te_3 glass, (triangles) data from [22] and (circles) data from [20] for (solid symbols) increasing and (open symbols) decreasing pressure, in comparison with our results (solid lines). The gray dashed line indicates a resistivity level of 10^3 Ω cm, which corresponds to the Mott criterion of metallization.

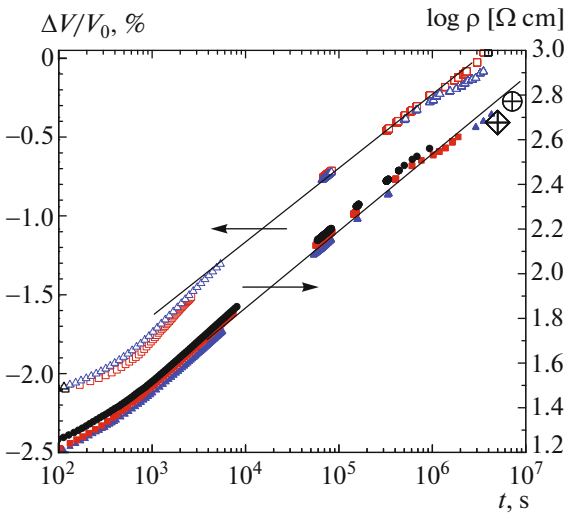

Fig. 8. (Color online) Relaxation of the volume and the electrical resistivity of the g-As_2Te_3 glass after pressure release. (large symbols) Results of measuring the electrical resistivities of two samples remaining after measuring $V(P)$ and volume relaxation.

of the relaxed hot-pressed samples. Figure 8 shows the time dependences of the volume and the electrical resistivity of the samples under normal conditions. It is interesting that the logarithmic relaxation of both density and electrical resistivity is observed over a wide time range with a possible tendency toward saturation at times longer than 10^7 s (see Fig. 8).

It was also interesting to compare the rate of change of the electrical resistivity referred to a fixed change in the volume (by, e.g., 1%) under various conditions. It was found that the rate of change of the electrical resistivity as a function of volume during an increase and decrease in the pressure is substantially lower than during isobaric relaxation (Fig. 9). For example, an increase in the density by 1% during compression at the maximum pressures leads to a decrease in the electrical resistivity by 25%, whereas the same increase in the density during isobaric holding corresponds to a twofold decrease in the electrical resistivity. When the force decreases in the minimum pressure range, the increase in the electrical resistivity caused by a decrease in the density by 1% is 70–120%, whereas this increase is 570% during relaxation under normal pressure. These data demonstrate that substantial part of the relaxation processes occurs without changing the density.

To interpret the experimental data on compressibility and electrical resistivity, we performed comparative structural studies of the quenched and hot-pressed glasses and the samples subjected to high pressure. The structural studies were carried out approximately one moth after preparing these glasses. The structure factors of all three groups of glasses are very close to each other. The typical neutron ($S_N(Q)$) and X-ray ($S_X(Q)$) structure factors of glassy As_2Te_3 were shown above in Fig. 1. These factors almost coincide with the reported factors. Clear oscillations at large superconducting vectors $Q \geq 20$ Å^{-1} are visible in the curves of reduced structure factor $Q[S_i(Q) - 1]$, where $i = N$ or X, which indicates a stable local order in g-As_2Te_3. The main feature of the $S_N(Q)$ and $S_X(Q)$ dependences at small scattering vectors $Q < 5$ Å^{-1} is the first sharp diffraction peak (FSDP), the position of which is different for X-ray diffraction and neutron diffraction measurements (Fig. 10a),

$$Q_0(N) = 1.15 \pm 0.04 \text{ Å}^{-1},$$
$$Q_0(X) = 1.28 \pm 0.02 \text{ Å}^{-1}.$$

This large difference between the FSDP positions can be a significant chemical disorder in g-As_2Te_3 [3–9, 15–17] and different sensitivities of tellurium and arsenic to electromagnetic and nuclear radiation,

$$Z_{Te}/Z_{As} = 1.576, \quad \bar{b}_{Te}/\bar{b}_{As} = 0.881,$$

where Z_j and $\bar{b}_j$ correspond to the atomic number and the coherent length of neutron scattering of element j.

The most pronounced differences for the three groups of glasses are mainly related to the first FSDP, which demonstrates a clear shift (+0.05 Å^{-1}) toward high Q, a more pronounced asymmetry, and a lower amplitude after processing by hydrostatic pressure (see

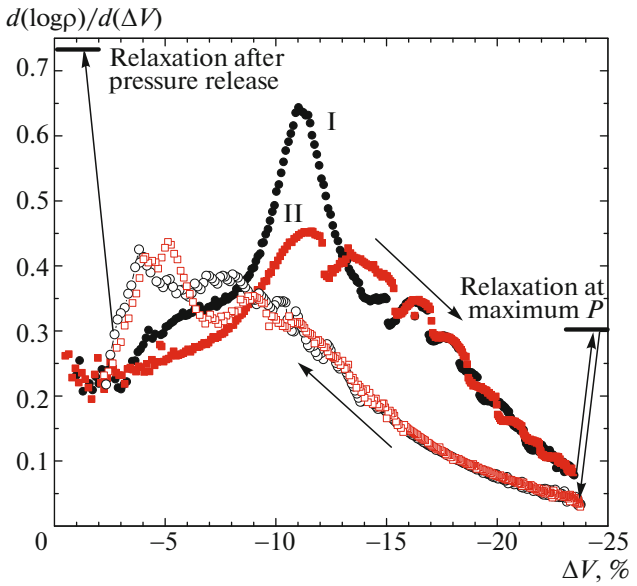

Fig. 9. (Color online) Derivatives of the electrical resistivity as a function of the volume change (in percentage of $\Delta V/V_0$)) for (I) quenched and (II) hot-pressed samples. The curves were obtained by calculating the data of two experiments (Fig. 6) from the averaged $V(P)$ dependences (Fig. 2) for (solid symbols) increasing and (open symbols) decreasing pressure. The colors and symbols designating different experiments coincide with those in Fig. 6. The points at the end of the reverse run (at $\Delta V < 10\%$) are strongly smoothed. It is impossible to plot electrical resistivity as a function of volume correctly in this range because of strong volume and electrical resistivity correlations. The derivatives during relaxation at the maximum pressure and after pressure release, which were obtained as the ratio of the steady relaxation rates of electrical resistivity and volume, are also indicated in the curve.

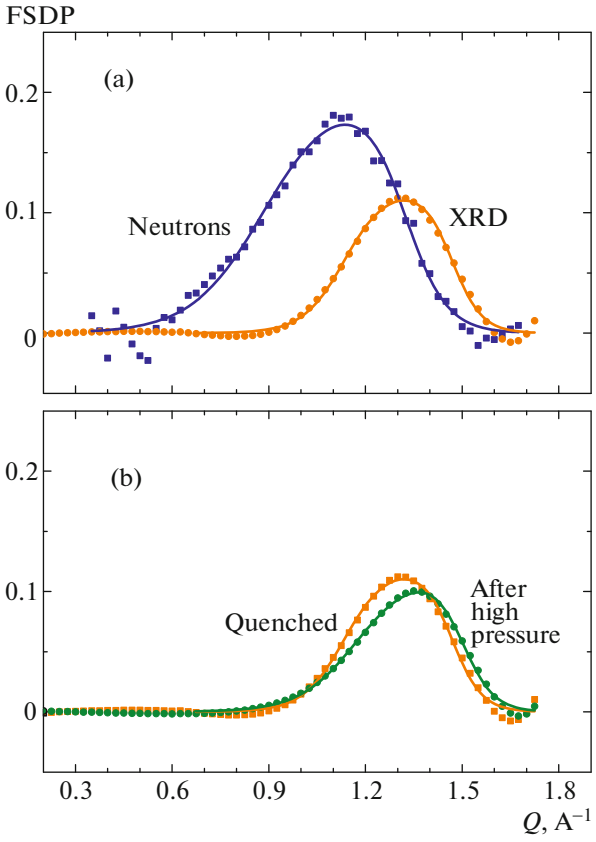

Fig. 10. (Color online) (a) FSDP of the quenched g-As_2Te_3 glass obtained from neutron diffraction and XRD data. (b) Effect of high pressure on the XRD FSDP in glassy As_2Te_3.

Fig. 10b). The results of a detailed analysis of the structural data obtained for the three groups of glasses are presented in Fig. 11, which shows total correlation functions obtained from structure factors (see below).

Figure 12 displays the Raman spectra of the following two types of samples: the quenched samples and the sample subjected to high-pressure treatment. These spectra were recorded approximately one year after sample preparation. A small but clear difference between these spectra is visible: it is larger than the statistical error by three times (see below).

Finally, the temperature dependences of the electrical resistivities of all three types of glasses were measured at normal pressure near room temperature (Fig. 13). It is seen that the quenched glasses have the highest electrical resistivity and the highest effective activation energy and the glasses subjected to high-pressure treatment have the lowest electrical resistivity. In addition, the temperature dependences of the latter glasses are characterized by strong time relaxation.

4. DISCUSSION AND CONCLUSIONS

The results obtained allow us to draw some conclusions regarding the behavior of the g-As_2Te_3 glasses during compression, their metallization, and the differences between the structures and properties of three groups of glasses (quenched, hot-pressed, and subjected to high-pressure treatment). We first discuss the structure and dynamics of the three groups of glasses.

The position of FSDP makes it possible to estimate the characteristic length of the intermediate-range order in the g-As_2Te_3 glass, $L \approx 2\pi/Q_0 = 4.9$–5.5 Å. These characteristic lengths in glassy arsenic sulfides and selenides are associated with the periodic repeatability of intermediate-range As–As correlations in the glass network, which are related to As_nX_n ($n < 20$) rings. The As_6X_6 (X = S, Se) rings in crystalline As_2S_3 and As_2Se_3 are a single intermediate-range element, in contrast to crystalline arsenic telluride [37–39]. Unfortunately, as noted above, a detailed description of the disordered network in g-As_2Te_3 and structural models for this glass have not been developed to date.

The Fourier transform with the Lorch function [40] gives the total correlation functions in real space

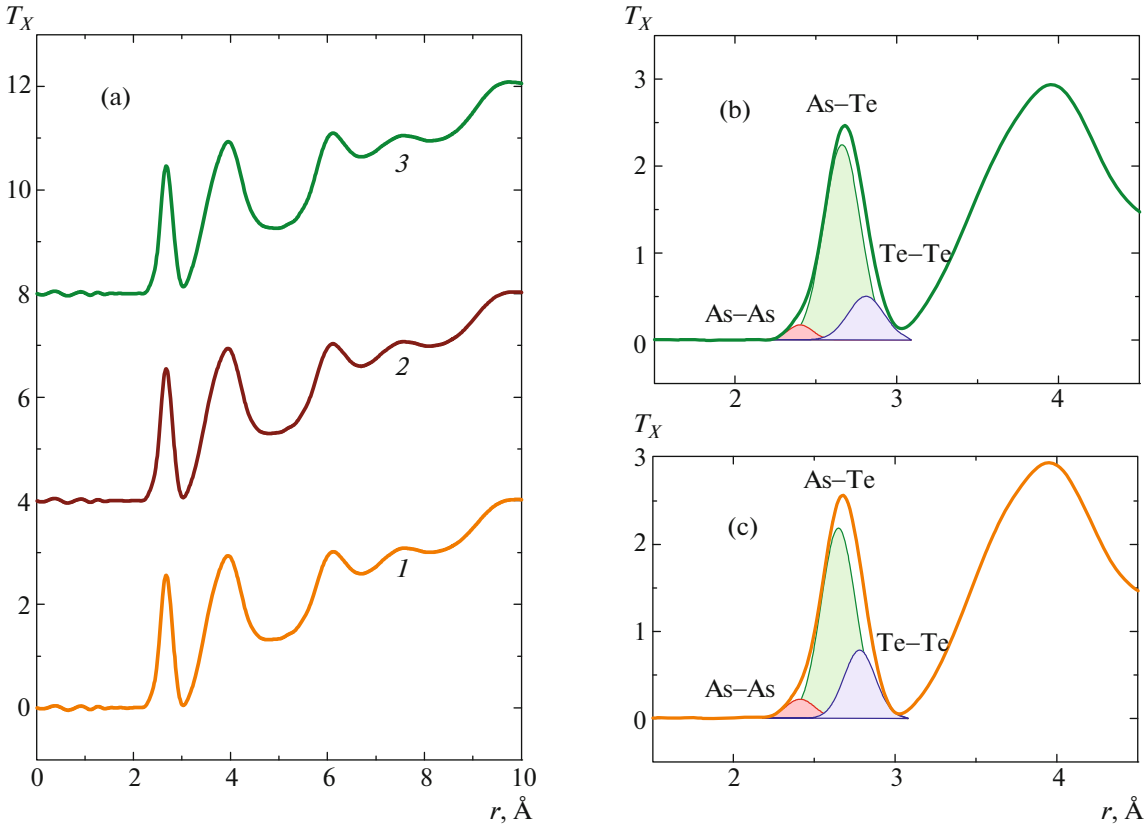

Fig. 11. (Color online) (a) X-ray total correlation functions $T_X(r)$ for (*1*) quenched As_2Te_3 glass, (*2*) hot-pressed glass (0.2 GPa, 136°C), and (*3*) after a cycle with a maximum pressure of 8.3 GPa. Typical processing of the nearest-neighbor peak of glassy As_2Te_3 (b) after treatment at a pressure of 8.3 GPa and (c) in the quenched sample. Designations As–As, As–Te, and Te–Te correspond to the nearest neighbors spaced 2.40, 2.65, and 2.80 Å apart, respectively.

that are shown in Fig. 11. The first asymmetric peak at 2.65 Å corresponds to the nearest neighbors in the glass network. The next-nearest and farther neighbors are characterized by the next peaks in the $T_X(r)$ curves at 4, 6, 7.5, and 9.5 Å. The asymmetric profile of the nearest-neighbor peak corresponds to several types of interatomic correlations. The pronounced broadening of the peak at $r \approx 2.40$ Å points to As–As correlations and, hence, a chemical disorder in the stoichiometric As_2Te_3 glass. The appearance of "wrong" bonds is associated with partial dissociation of arsenic telluride in the melt, which is approximately described by the simplified equilibrium

$$As_2Te_3 \rightleftarrows 2As + 3Te,$$

or, in terms of chemical bonds [8],

$$2As{-}Te \rightleftarrows As{-}As + Te{-}Te.$$

Thus, the nearest-neighbor peak should also include Te–Te correlations. The processing of the poorly resolved peak using three Gaussians without external limitations gives no stable solution. A reasonable hypothesis consists in fixing the total number coordination number of arsenic,

$$N_{As-X} = N_{As-As} + N_{As-Te} = 3,$$

which is supported by the results of EXAFS and anomalous X-ray scattering at the *K* edge of arsenic [3, 6]. This limitation ensures stable fitting results (see Fig. 11b, 11c, and Table 1).

On the whole, the obtained interatomic distances and the coordination numbers agree with the well-known reported data for the As–Te glasses and melts at atmospheric pressure. It should be noted that the total coordination number of tellurium is slightly larger than two, which indicates the presence of 10–15% three-coordinated tellurium in the glass network. However, the basic result is that the chemical disorder in glassy As_2Te_3 decreases after thermal and, especially, baric action (see Table 1). This result seems to be unexpected, since an increase in the chemical disorder at a high pressure and the related glass metallization would be expected. In particular, the main hypothesis associated with the existence of a significant chemical disorder in glassy As_2Te_3 is based on the metallization of the glass-forming melt at the tem-

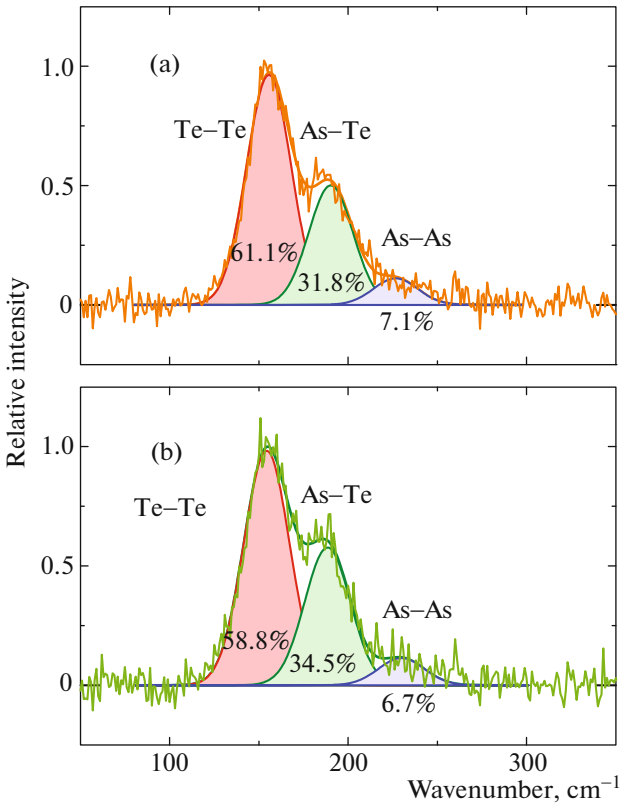

Fig. 12. (Color online) Typical Raman spectra of (a) quenched glass and (b) g-As_2Te_3 glass after a cycle with a maximum pressure of 8.3 GPa. The symmetric stretching vibrations at 150 (Te–Te), 190 (As–Te), and 230 (As–As) cm^{-1} are red, green, and blue, respectively.

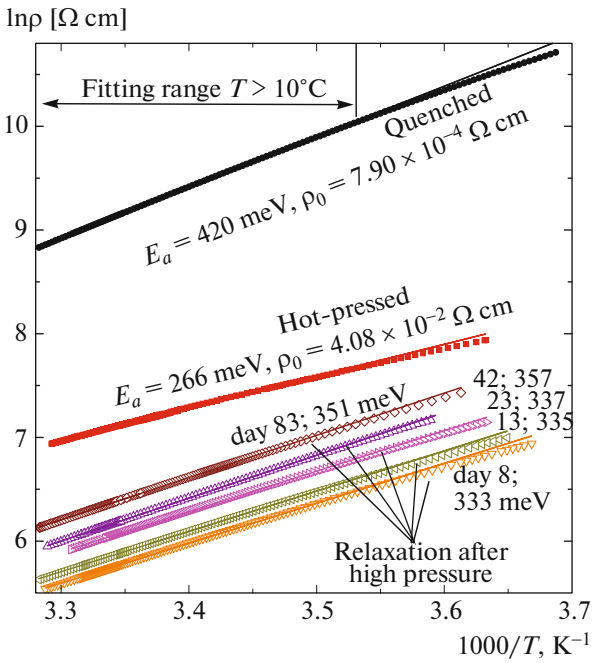

Fig. 13. (Color online) Temperature dependences of the electrical resistivity of g-As_2Te_3 glass samples measured (solid symbols) before performing experiments under pressure and (open symbols) after pressure release. In the latter case, only several dependences for two samples are shown to demonstrate a general tendency and the characteristic scales of relaxation processes (E_a is the activation energy).

peratures that are slightly higher than the liquidus temperature [15–17]. We shall dwell on this problem later.

The Raman spectroscopy of the quenched glasses and the glasses subjected to high-pressure treatment is an additional test of the results obtained. Figure 12 shows the typical Raman spectra of two types of samples. As follows from [8, 41–43], these spectra demonstrate the presence of the following three fundamental modes: symmetric stretching vibrations of Te–Te at 155 cm^{-1}, As–Te at 190 cm^{-1}, and As–As at 230 cm^{-1}. As in the case of XRD data, the simultaneous presence of these three stretching vibrations in the spectrum of the stoichiometric glass points to a significant chemical disorder. Here, the intensity of the "wrong" stretching vibrations (As–As, Te–Te) in the quenched glass is higher than that in the sample subjected to high-pressure treatment (even a year after treatment), which agrees with the XRD data.

Thus, an analysis of the structural and Raman spectroscopy results demonstrates that the samples

Table 1. Structural parameters (nearest interatomic distances, partial coordination numbers) of glassy As_2Te_3: I, quenched; II, hot-pressed; and III, after high pressure

Sample	As—As		As–Te		Te–Te		$N_{Te-(As-Te)}$	Chemical disorder
	r, Å	N_{As-As}	r, Å	N_{As-Te}	r, Å	N_{Te-Te}		
I	2.41	0.64	2.65	2.36	2.78	0.53	2.10	0.21
II	2.40	0.53	2.65	2.47	2.78	0.51	2.16	0.18
III	2.40	0.43	2.65	2.57	2.81	0.44	2.15	0.14

The chemical disorder was determined as the ratio of the number of homopolar As–A bonds to the total number of As–Te and As–As bonds, $N_{As-As}/(N_{As-As} + N_{As-Te})$. The average standard deviations of the calculated parameters are ±0.01 Å for the As–As and As–Te bond lengths and ±0.02 Å for Te–Te. The corresponding errors for the coordination numbers are ±0.02 for N_{As-As} and N_{As-Te} and ±0.04 for N_{Te-Te}.

subjected to high-pressure treatment have the minimum chemical disorder, the quenched glasses have the maximum chemical disorder, and the hot-pressed glasses have an intermediate disorder (see Figs. 11b, 11c, 12; Table 1). At first glance, this finding contradicts intuition, since the pressure-induced metallization usually decreases the covalence and increases the chemical disorder. On the other hand, however, the rapid decrease in the glass transition temperature and the crystallization temperature with increasing pressure should substantially accelerate local diffusion during compression [24]. At a pressure of 4–6 GPa, the softening and crystallization temperatures of the glass can be slightly higher than room temperature. The application of pressure is assumed to heal defects and a chemical disorder more intensely than annealing of glasses at low pressures. A microscopic mechanism of this ordering during a structural transition can be described as follows. The potential energy of "wrong" network atoms should be slightly higher than that of "regular" atoms. Therefore, the corresponding barriers are slightly lower and, hence, the probability of a wrong-atom jump to a new site during restructuring of the network can be higher than that of a regular-atom jump.

Another counterintuitive finding is that samples with a lower chemical disorder have a lower electrical resistivity (see Fig. 13). We assume that a large number of wrong neighbors and defects leads to a high degree of carrier localization and to an increase in the energy gap because of a decrease in the carrier mobility despite a formally high degree of metallization (number of Te–Te neighbors). As an indirect supporting argument, we note that the quenched samples have an electrical resistivity of 9.9×10^3 Ω cm, an activation energy $E_a = 420$ eV, and an effective electrical resistivity $\rho_0 = 7.9 \times 10^{-4}$ Ω cm, whereas the hot-pressed samples have the electrical resistivity that is lower by an order of magnitude (1.25×10^3 Ω cm at $T = 25$°C) but a significantly lower activation energy (E_a = 266 meV) and, hence, the effective electrical resistivity that is higher by almost two orders of magnitude ($\rho_0 = 4.1 \times 10^{-2}$ Ω cm). Note that these values of E_a correspond to the temperature range 10–30°C, the dependence $\ln\rho(1/T)$ is substantially nonlinear, and the apparent energy gap increases with temperature.

Moreover, the behavior of the density and, especially, the electrical resistivity of the samples subjected to high-pressure treatment demonstrates that they relax intensely under normal conditions (see Figs. 8, 13). Obviously, the structures of these samples depend substantially on time. Recall that the structural investigations of all three types of samples were carried out approximately a month from preparation and that the Raman spectroscopy studies were performed almost a year after sample preparation. Obviously, it is impossible to compare the fractions of wrong bonds quantitatively in samples with different histories.

As for the behavior of the g-As_2Te_3 glasses during compression, the anomalies of their density and electrical resistivity in the pressure range 2–3.5 GPa are unambiguous manifestation of polyamorphism. However, the small volume anomaly (about 2%) and coincident relaxed bulk moduli in the direct and reverse runs of curves point to an almost unchanged structure of the short-range order in the glasses (in contrast to, e.g., g-GeO_2 glasses [33]) and to an unchanged average coordination number. Compression is assumed to be accompanied by a change in the intermediate-range order, including the type of connection of polyhedra, and by chemical ordering (disordering).

Note that the sharp softening of the effective bulk modulus of the g-As_2Te_3 glasses at a pressure of 2–2.5 GPa resembles the behavior of the g-$GeSe_2$ glasses [34]. We suppose that, as in the case of the g-$GeSe_2$ glasses, the local elastic constants of the structural units formed by edge-sharing $AsTe_{3/2}$ pyramids (tetrahedra for $GeSe_2$) are softened. The amorphous network of the g-As_2Te_3 glasses is based on both edge-sharing and vertex-sharing $AsTe_{3/2}$ pyramids (detailed structural model will be considered at the end of the article). The intense relaxation processes that occur in the g-As_2Te_3 glasses at a pressure of 2–2.5 GPa are likely to be related to a change in the type of connection of pyramids from edge-sharing connection to corner-sharing connection (this fact was established for the case of g-$GeSe_2$). Polyamorphism is accompanied by a very sharp decrease in the electrical resistivity, an almost three orders of magnitude, when pressure changes from 2 to 3.5 GPa. Nevertheless, substantial differences in the behaviors of these two glasses take place. For the g-$GeSe_2$ glasses, the leveling off and the subsequent softening of the elastic moduli in the pressure range 1.5–3 GPa occur elastically without relaxation, and intense relaxation processes begin only when the pressure increases further (in the range 3–5 GPa). The relaxation processes and the softening of the effective bulk modulus in the g-As_2Te_3 glasses begin almost simultaneously at a pressure above 1 GPa.

As a result of a low glass transition temperature and a high atomic mobility, the samples in the pressure range 3–3.5 GPa forget their history and the electrical resistivities of different initial (quenched and hot-pressed) samples have a common dependence (see Fig. 6). As the pressure increases further, the intermediate-range order is likely to change gradually, without substantial changes in coordination. The As_2Te_3 glasses undergo metallization at a pressure of 5 GPa, which is two times lower than it was considered earlier. As noted above, the high error in the measurements performed in [20, 22] was related to nonhydrostatic conditions and bad measuring contacts. The As_2Te_3 glasses are in a metallic state in a wide pressure range of 5–8.5 GPa.

The inflection point in the baric dependence of the relaxed bulk modulus when the pressure decreases near 4 GPa is interesting. We have not detected such an inflection point in the oxide and chalcogenide glasses studied earlier (see, e.g., [33–35]). In this pressure range, no structural transformations and relaxation take place in the reverse run of the curves and the electrical resistivity is 5×10^{-4} Ω cm. This effect can be explained by an additional contribution of a free electron gas to the energy at pressures above 4 GPa (and electrical resistivity lower than 5×10^{-4} Ω cm). The electrical resistivity at this crossover is arbitrary to a certain extent. It is determined by the relative contribution of this additional metallic bond with respect to the covalent bond. Therefore, an electrical resistivity of 5×10^{-4} Ω cm can be considered as a metallization criterion. The "metallic" contribution to the interatomic interaction changes strongly with pressure: the electrical resistivity changes threefold in the metallic phase region during pressure release in the range 4–8 GPa. It is this finding that can explain the high baric derivative of the bulk modulus (which is higher by a factor of 8) in comparison with conventional metals, where the conduction electron concentration weakly depends on pressure.

The residual densification (about 2%) and the anomalously low electrical resistivity (about 10 Ω cm) right after pressure release are associated with partial irreversibility of transformation (apparently, a change in the type of connection of $AsTe_{3/2}$ pyramids). An amorphous network relaxes to a quasi-equilibrium state during long-term holding (10^7 s) under normal conditions.

The absence of structural models for glassy arsenic telluride hinders a detailed interpretation of the XRD and Raman spectroscopy results. In addition, the structure of crystalline As_2Te_3 differs strongly from that of auripigment, monoclinic As_2S_3 [37], its triclinic dimorph [38], and the selenide analog of auripigment (monoclinic As_2Se_3) [39]. Sulfide and selenide sesquichalcogenides As_2X_3 have a layered structure, where two-dimensional layers are formed by As_6X_6 rings and every arsenic atom belongs to three neighboring rings. A similar two-dimensional structure is retained in the glass; however, a single type of rings in crystals is replaced by their broad distribution [44]. The monoclinic lattice of α-As_2Te_3, which is stable at atmospheric pressure, is formed by $(As_4Te_6)_\infty$ bands, where arsenic atoms occupy octahedral (As(2)) and trigonal (As(1)) sites with a broad distribution of interatomic distances (2.82 ± 0.11 Å) [45–48]. The interatomic distances in liquid and glassy arsenic tellurides are substantially smaller, 2.65 ± 0.03 Å (see Table 1) [3–17]. This means that the topology of the crystal lattice changes in melting and gives an alternative system of bonds.

As a working hypothesis, we consider the formation of two chemically ordered motifs in the glass network, which are related to the transformation of $(As_4Te_6)_\infty$ bands (Fig. 14). When limiting chemically bounded/unbounded atomic pairs at 2.85 Å, an $(As_4Te_6)_\infty$ band decomposes into the following three chains: a central chain consisting of edge-sharing ES–$AsTe_{3/3}$ pyramids and two lateral chains consisting of corner-sharing CS–$AsTe_{2/3}$ structural units. The central motif of the transformation is as follows: ES–$AsTe_{3/3}$ loses every third arsenic atom and transforms into the chain consisting of alternate edge- and corner-sharing $AsTe_{3/2}$ pyramids (Fig. 14c). The two lateral chains with the remaining arsenic atoms are joined together to form a new As–Te band consisting of As_3Te_3 and As_6Te_6 rings (Fig. 14d).

The topological and structural disorders in a melt and, then, glass inevitably cause a ring size distribution similarly to glassy arsenic sulfides and selenides. The extremely close binding energies of As–As (134.2 kJ/mol), As–Te (137.0 kJ/mol), and Te–Te (137.9 kJ/mol) [49]; partial dissociation of As–Te at finite temperatures; and melt metallization would be responsible for the chemical disorder in the glasses.

This hypothesis is supported by available experimental data. The FSDP in the neutron diffraction and XRD results evidences that intermediate-range As–As correlations are present in glassy As_2Te_3, as those in sulfide and selenide glasses. In particular, this also follows from FSDP amplitudes $A_0(N)$ and $A_0(X)$ in the neutron and X-ray structure factors. The ratio $A_0(N)/A_0(X) = 1.7$ is close to the ratio $W_{AsAs}(N)/W_{AsAs}(X) = 2.5$. Here, $W_{AsAs}(N)$ and $W_{AsAs}(X)$ correspond to the neutron and X-ray weight coefficients of the As–As correlations in determining $S_N(Q)$ and $S_X(Q)$ using the Faber–Ziman formalism [50],

$$S_N(Q) - 1 = \Sigma_{ab} W_{ab}(N)[S_{ab}(Q) - 1]$$
$$= \Sigma_{ab} c_a c_b \frac{\bar{b}_a \bar{b}_b}{|\Sigma_a c_a \bar{b}_a|^2}[S_{ab}(Q) - 1],$$
$$S_X(Q) - 1 = \Sigma_{ab} W_{ab}(N)[S_{ab}(Q) - 1]$$
$$= \Sigma_{ab} c_a c_b \frac{f_a(Q) f_b(Q)}{|\Sigma_a c_a \bar{b}_a|^2}[S_{ab}(Q) - 1],$$

where the values of $S_{ab}(Q)$ correspond to the partial structure factors of the atomic pairs As–As, As–Te, and Te–Te and $f_a(Q)$ is the Q-dependent X-ray atomic scattering factor of element a ($f_a(0) = Z_a$). Both the numerical differences and different FSDP positions $Q_0(N)$ and $Q_0(X)$ are related to the second contribution to the FSDP from the Te–Te correlations, which are more pronounced in the XRD data, $W_{TeTe}(N)/W_{TeTe}(X) = 0.6$. The intermediate-range As–As correlations are determined by the statistics of As_nTe_n rings, as in the g-As_2S_3 or g-As_2Se_3 glasses. Our

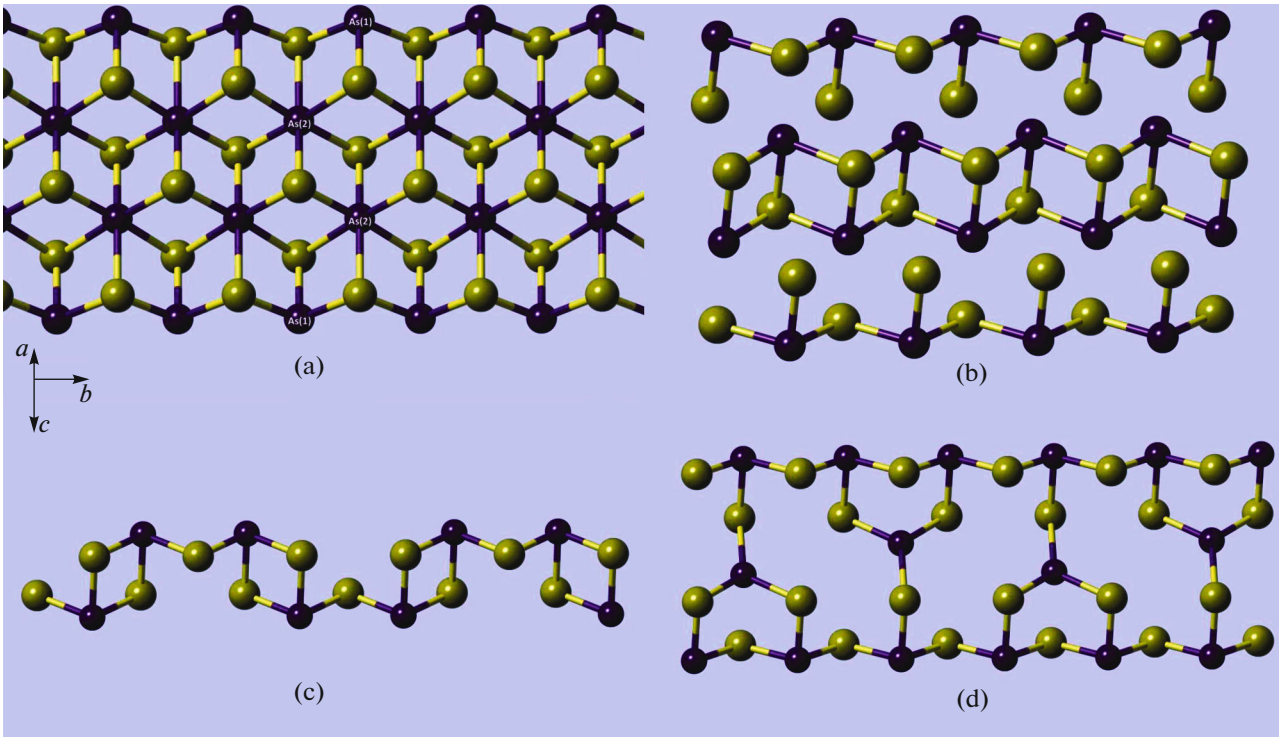

Fig. 14. (Color onlime) Hypothetic transformation of the $(As_4Te_6)_\infty$ band in crystalline α-As_2Te_3 with the formation of two chemically ordered motifs in glassy g-As_2Te_3: (a) isolated $(As_4Te_6)_\infty$ band contains octahedral (As(2)) and trigonal (As(1)) arsenic sites with a broad distribution of As–Te interatomic distances (2.82 ± 0.11 Å). (b) Limit "chemically bound (nearest)/unbound (next-nearest) As–Te neighbors" is found at 2.85 Å; an isolated $(As_4Te_6)_\infty$ band decomposes into the following three chains: a central chain consisting of edge-sharing ES–$AsTe_{3/3}$ pyramids and two lateral chains consisting of corner-sharing CS–$AsTe_{2/3}$ structural units. The central motif ES–$AsTe_{3/3}$ loses every third arsenic atom and transforms into chain (c) consisting of alternate edge- and corner-sharing $AsTe_{3/2}$ pyramids. (d) The two lateral chains with the remaining arsenic atoms are joined together to form a new As–Te band consisting of As_3Te_3 and As_6Te_6 rings.

preliminary results on a structural simulation of glassy arsenic telluride, which were obtained by the density functional theory (DFT) and the reverse Monte Carlo (RMC) method, support the analysis of the behavior of the FSDP prepeak. Nevertheless, the cause of decreasing the chemical disorder after baric action is still an open question and requires both X-ray diffraction and spectroscopic in situ structural measurements.

Thus, using high-precision measurements of the volume and the electrical resistivity of the g-As_2Te_3 glasses at a certain pressure under hydrostatic conditions, we were able to reveal the main features of the transformations in them. We revealed the following clear pressure ranges: up to 1 GPa, normal linear behavior; from 1 to 2 GPa, beginning of inelastic behavior; from 2 to 3.5 GPa, polyamorphic transformation accompanied by a strong softening of the effective bulk modulus and intense logarithmic density relaxation; and from 3.5 to 8.5 GPa, inelastic behavior with moderate relaxation and gradual metallization at 5 GPa. The diffuse transformation in the glasses is only partly reversible.

For a further investigation of the polyamorphism and metallization in the g-As_2Te_3 glasses, it is desirable to perform detailed structural studies under pressure and ab initio calculations. However, as noted above, the data on the short-range and intermediate-ranges orders in the g-As_2Te_3 glasses are conflicting even at normal pressure. The simulation of the structure of the g-As_2Te_3 glasses also did not result in satisfactory agreement with experimental data. In this work, we only give some preliminary considerations to the structural motifs in these glasses and their possible change in compression. This work is thought to be a stimulus to a comprehensive experimental and theoretical investigation of the structure and the dynamics of the g-As_2Te_3 glasses at normal and high pressures.

ACKNOWLEDGMENTS

We thank Dr. C.J. Benmore for his help in the high-energy diffraction measurements. The work on the Advanced Photon Source (Argonne National Laboratory) was supported in part by the Basic Research Office of the Department of Energy of the United

States. We thank N.F. Borovikov and I.P. Zibrov for their assistance with performing the chemical and phase analyses of samples.

This work was supported by the Russian Science Foundation, project no. 14-22-00093.

REFERENCES

1. M. Wuttig and N. Yamada, Nat. Mater. **6**, 824 (2007).
2. J. Cornet and D. Rossier, J. Non-Cryst. Solids **12**, 85 (1973).
3. Q. Ma, D. Raoux and S. Benazeth, Phys. Rev. B **48**, 16332 (1993).
4. K. Abe, O. Uemura, T. Usuki, et al., J. Non-Cryst. Solids **232–234**, 682 (1998).
5. G. Faigel, L. Granasy, I. Vincze, and H. de Waard, J. Non-Cryst. Solids **57**, 411 (1983).
6. P. Jóvári, S. N. Yannopoulos, I. Kaban, et al., J. Chem. Phys. **129**, 214502 (2008).
7. S. Sen, S. Joshi, B. G. Aitken, and S. Khalid, J. Non-Cryst. Solids **354**, 4620 (2008).
8. A. Tverjanovich, K. Rodionov, and E. Bychkov, J. Solid State Chem. **190**, 271 (2012).
9. D. C. Kaseman, I. Hung, K. Lee, et al., J. Phys. Chem. B **119**, 2081 (2015).
10. M. Dongol, T. Gerber, M. Hafiz, et al., J. Phys.: Condens. Matter **18**, 6213 (2006).
11. T. G. Edwards, E. L. Gjersing, S. Sen, et al., J. Non-Cryst. Solids **357**, 3036 (2011).
12. M. Tenhover, P. Boolchand, and W. J. Bresser, Phys. Rev. B **27**, 7533 (1983).
13. S. S. K. Titus, R. Chatterjee, S. Asokan, and A. Kumar, Phys. Rev. B **48**, 14650 (1993).
14. S. Sen, S. Soyer Uzun, C. J. Benmore, and B. J. Aitken, J. Phys.: Condens. Matter **22**, 405401 (2010).
15. A. Tverjanovich, M. Yagodkina, and V. Strykanov, J. Non-Cryst. Solids **223**, 86 (1998).
16. H. Endo, H. Hoshino, H. Ikemoto, and T. Miyanaga, J. Phys.: Condens. Matter **12**, 6077 (2000).
17. C. Otjacques, J. Raty, F. Hippert, et al., Phys Rev. B **82**, 054202 (2010).
18. G. Parthasarathy and E. S. R. Gopal, Bull. Mater. Sci. **7**, 271 (1985).
19. S. Minomura, in *Amorphous Semiconductors: Technologies and Devices*, Ed. by Y. Hamakawa (North Holland, Amsterdam, 1978), p. 245.
20. N. Sakai and H. Fritzsche, Phys. Rev. B **15**, 973 (1977).
21. I. V. Berman, N. V. Brandt, I. E. Kostyleva, et al., JETP Lett. **43**, 62 (1986).
22. G. Ramani, A. Giridhar, and A. K. Singh, Philos. Mag. B **39**, 385 (1979).
23. J. Kristofic, J. J. Mares, and V. Smid, Phys. Status Solidi A **89**, 333 (1985).
24. K. Ramesh, J. Phys. Chem. B **118**, 8848 (2014).
25. C. J. Benmore and A. K. Soper, *The SANDALS Manual: A Guide to Performing Experiments on the Small Angle Neutron Diffractometer for Amorphous and Liquid Samples at ISIS* (Rutherford-Appleton Labor., 1998).
26. A. C. Hannon, W. S. Howells, and A. K. Soper, Inst. Phys. Conf. Ser. **107**, 193 (1990).
27. O. L. G. Alderman, M. Liška, J. Macháček, et al., J. Phys. Chem. C **120**, 553 (2016).
28. A. P. Hammersley, S. O. Svensson, M. Hanfland, et al., High Press. Res. **14**, 235 (1996).
29. C. N. J. Wagner, J. Non-Cryst. Solids **31**, 1 (1978).
30. L. B. Skinner, C. J. Benmore, and J. B. Parise, Nucl. Instr. Methods Phys. Res. A **662**, 61 (2012).
31. L. G. Khvostantsev, V. N. Slesarev, and V. V. Brazhkin, High Press. Res. **24**, 371 (2004).
32. O. B. Tsiok, V. V. Bredikhin, V. A. Sidorov, and L. G. Khvostantsev, High Press. Res. **10**, 523 (1992).
33. O. B. Tsiok, V. V. Brazhkin, A. G. Lyapin, and L. G. Khvostantsev, Phys. Rev. Lett. **80**, 999 (1998).
34. V. V. Brazhkin, E. Bychkov, and O. B. Tsiok, Phys. Chem. B **120**, 358 (2016).
35. V. V. Brazhkin, O. B. Tsiok, and J. Katayama, JETP Lett. **89**, 244 (2009).
36. V. V. Struzhkin, A. F. Goncharov, R. Caracas, et al., Phys. Rev. B **77**, 165133 (2008).
37. D. J. E. Mullen and W. Nowacki, Z. Kristallogr. **136**, 48 (1972).
38. A. R. Kampf, R. T. Downs, R. M. Housley, et al., Miner. Mag. **75**, 2857 (2011).
39. A. C. Stergiou and P. J. Rentzeperis, Z. Kristallogr. **173**, 185 (1985).
40. E. Lorch, J. Phys. C **2**, 229 (1969).
41. J. S. Lannin, Phys. Rev. B **15**, 3863 (1977).
42. J. R. Magana and J. S. Lannin, Phys. Rev. Lett. **51**, 2398 (1983).
43. A. Mendoza-Galvan, E. Garcıa-Garcıa, Y. V. Vorobieva, and J. Gonzalez-Hernandez, Microelectron. Eng. **51–52**, 677 (2000).
44. S. I. Simdyankin, S. R. Elliott, Z. Hajnal, et al., Phys. Rev. B **69**, 144202 (2004).
45. G. J. Carron, Acta Crystallogr. **16**, 338 (1963).
46. A. S. Kanishcheva, Yu. N. Mikhailov, and A. P. Chernov, Neorg. Mater. **18**, 949 (1982).
47. A. C. Stergiou and P. J. Rentzeperis, Z. Kristallogr. **172**, 139 (1985).
48. C. Morin, S. Corallini, J. Carreaud, et al., Inorg. Chem. **54**, 9936 (2015).
49. M. Deli, D. Houphouet Boigny, and G. Kra, J. Non-Oxide Glasses **1**, 59 (2010).
50. T. E. Faber and J. M. Ziman, Philos. Mag. **11**, 153 (1965).

Translated by K. Shakhlevich